Simulation optimization of spherical non-polar guest recognition by deep-cavity cavitands

Piyush P. Wanjari,[1] Bruce C. Gibb,[2] and Henry S. Ashbaugh[1,a)]
[1]*Department of Chemical and Biomolecular Engineering, Tulane University, New Orleans, Louisiana 70118, USA*
[2]*Department of Chemistry, Tulane University, New Orleans, Louisiana 70118, USA*

(Received 5 August 2013; accepted 22 November 2013; published online 17 December 2013)

Biomimetic deep-cavity cavitand hosts possess unique recognition and encapsulation properties that make them capable of selectively binding a range of non-polar guests within their hydrophobic pocket. Adamantane based derivatives which snuggly fit within the pocket of octa-acid deep cavity cavitands exhibit some of the strongest host binding. Here we explore the roles of guest size and attractiveness on optimizing guest binding to form 1:1 complexes with octa-acid cavitands in water. Specifically we simulate the water-mediated interactions of the cavitand with adamantane and a range of simple Lennard-Jones guests of varying diameter and attractive well-depth. Initial simulations performed with methane indicate hydrated methanes preferentially reside within the host pocket, although these guests frequently trade places with water and other methanes in bulk solution. The interaction strength of hydrophobic guests increases with increasing size from sizes slightly smaller than methane to Lennard-Jones guests comparable in size to adamantane. Over this guest size range the preferential guest binding location migrates from the bottom of the host pocket upwards. For guests larger than adamantane, however, binding becomes less favorable as the minimum in the potential-of-mean force shifts to the cavitand face around the portal. For a fixed guest diameter, the Lennard-Jones well-depth is found to systematically shift the guest-host potential-of-mean force to lower free energies, however, the optimal guest size is found to be insensitive to increasing well-depth. Ultimately our simulations show that adamantane lies within the optimal range of guest sizes with significant attractive interactions to match the most tightly bound Lennard-Jones guests studied. © *2013 AIP Publishing LLC*. [http://dx.doi.org/10.1063/1.4844215]

INTRODUCTION

Octa-acid (OA) is a water soluble, deep-cavity cavitand that possesses a water-soluble outer coat and a deep hydrophobic pocket suitable for binding a range of guest molecules (Figure 1).[1,2] The water-soluble coat of OA is comprised of eight carboxylic acid groups bestowing the host with good solubility above pH ∼8. The interior hydrophobic pocket approximates to a truncated cone roughly 8 Å wide at its mouth, 3 Å wide at its base, and 8 Å deep. Two other features of the pocket impact the properties of OA. First, the four benzal hydrogens pointing into the cavity at its midsection pinch the cone somewhat and offer weak hydrogen bond donors to resident guests.[3] Second, the pocket entrance is rimmed with aromatic rings that bestows OA a predisposition to assemble into dimeric capsules.[4] These capsules have been used as yoctoliter reaction vessels,[5–7] separation devices,[8,9] for modulating the properties of redox-active[10] or fluorescence guests,[11,12] as well as controlling electron transfer[13] and electron–electron communication.[14] In addition to this capsule chemistry, three classes of guests bind to OA without triggering assembly and consequently allow the study of a range of 1:1 complexes. These classes of guest represent a wide diversity; small hydrophobic molecules,[8] amphiphiles such as long-chain fatty acids,[15] and chaotropic anions[16] all have an affinity for the hydrophobic pocket. As such, OA and related cavitands are interesting synthetic targets for mimicking ligand recognition in protein clefts.

The interaction free energies between non-polar species in water are typically understood to be dominated by favorable entropies of association,[17] frequently ascribed to the release of orientationally restricted waters from overlapping hydration shells. Recent experiments of ligand interactions with protein hydrophobic recognition pockets, however, indicate binding can be stabilized by enthalpy[18] and the pocket can be dry,[19] nullifying binding facilitated by water release. While molecular simulation studies of hydrophobic interactions have largely focused on the water-mediated interactions between small, spherical species which conform to entropically controlled association, such as methane,[20–23] more recent simulations of host-guest interactions driven by hydrophobic interactions have focused on the aqueous binding of idealized convex hydrophobic guests with concave hydrophobic pockets and clefts.[24,25] These simulations find the interaction between a spherical hydrophobe with a concave pocket is more strongly favored by the enthalpy of association. This enthalpic force has been attributed to the spontaneous escape of water from the pocket as the hydrophobic guest draws close, dewetting the pocket.[26] Simulations of

a)Author to whom correspondence should be addressed. Electronic mail: hanka@tulane.edu.

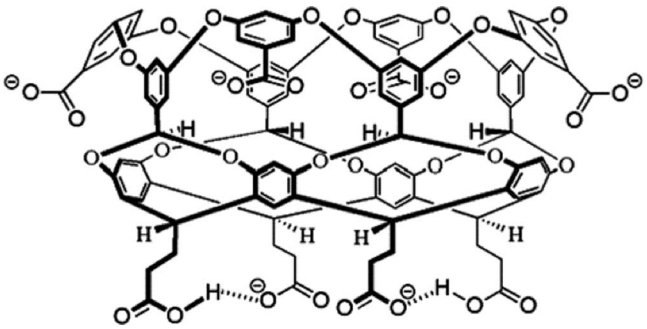

FIG. 1. Chemical structure of octa-acid deep-cavity cavitand host. The host possesses three rows of aromatic rings that build up the concave binding pocket. The mouth of the cavitand at the top of this structure is rimmed with four carboxylic acid coating groups that are presumed to be fully deprotonated at pH 7. The foot of the cavitand posses four carboxylic acid coating groups with only two presumed to be deprotonated at pH 7.

water within OA previously found that while 4 to 5 waters on average fill the hydrophobic pocket, the water occupancy fluctuates significantly from empty to up to 7 waters.[27] These simulations suggest water within the OA pocket lie on the verge of a liquid/vapor phase transition, in agreement with simulations of water penetration into carbon nanotubes.[28] Similar to pocket-like hosts, carbon nanotubes exhibit a strong affinity for the adsorption of hydrophobic species into their interiors.[29,30]

In an effort to better understand factors that determine hydrophobic guest selectivity by OA, we have conducted molecular simulations of cavitand host interactions with adamantane and a series of Lennard-Jones (LJ) guests to form 1:1 complexes in water. Adamantane is a nearly spherical hydrocarbon that snugly fits within cavitand pockets and its derivatives comprise a class of strongly binding compounds.[31,32] We aim to explore the effects of guest size and attractive interactions on optimal guest-host complexation. To map preferential hydrophobic guest binding sites, initial simulations examined the correlations between methanes and the host by allowing the guests to freely sample the cavitand's exterior and interior surfaces. Subsequent to verifying that the cavitand's non-polar pocket exerts the strongest binding preference, further simulations have focused on evaluating potentials-of-mean force (PMFs) between the pocket and a series of non-polar solutes to quantify the effects of guest size and attractiveness, manifested by the guest LJ diameter and well-depth, to sort binding selectivities. Breaking PMFs into direct guest-host interactions and indirect solvent-mediated contributions, we examine water's role in optimizing guest binding.

METHODS

Molecular dynamics simulations[33] of an OA deep-cavity cavitand host with a range of hydrophobic guests in aqueous solution were performed using the GROMACS 4.0 simulation package.[34] Water was modeled using the TIP4P-Ew potential.[35] The guests modeled were adamantane and a range of monatomic LJ solutes of varying size and attractiveness. The LJ, bond-length, angle-bending, and dihedral torsional interactions of adamantane and OA were modeled using the Generalized Amber Force Field.[36] Gaussian03 *ab initio* calculations were performed to optimize the geometries of adamantane and OA using the Hartree-Fock method and 6-31G* basis set.[37] The Antechamber module of AMBER 9[38] was subsequently used to assign AM1-BCC partial charges to the geometry-optimized molecules. Following Ewell, Gibb, and Rick,[27] six of the eight carboxylic acid coating groups of OA were assumed to be deprotonated at pH 7 imparting a net charge of $-6\ e$ to the cavitand host. Specifically, the four acids ringing the hydrophobic pocket at the top of OA and two acids diagonal to one another at the foot of OA were deprotonated (Figure 1). The carboxylic acid charges were neutralized by six sodium cations modeled using the AMBER 2003 force field. Non-bonded LJ interactions were truncated at a separation of 9 Å, with standard mean-field corrections for the energy and pressure applied beyond the cut-off. Cross LJ interactions between unlike species were determined using Lorentz-Berthelot combining rules.[33] Long-range electrostatic interactions were evaluated using the particle mesh Ewald method.[39] A time step of 2 fs was used to integrate the equations of motion. Simulations were conducted in the isothermal-isobaric ensemble at 300 K and 1 bar with the temperature and pressure controlled using the Nosé-Hoover thermostat[40,41] and Parrinello-Rahman barostat,[42] respectively. Bonds involving hydrogen were constrained using the LINCS algorithm.[43]

In a preliminary simulation to characterize the hydrophobic pocket of OA we examined the distribution of methanes about the cavitand in water. In this simulation one OA, 10 methanes, and 1500 water molecules were considered. The methanes, modeled using the OPLS united-atom LJ potential,[44] were free to explore the simulation box. The system was equilibrated for 10 ns followed by a 50 ns production run. System configurations were saved every 0.5 ps for evaluation of methane distributions.

In a second set of calculations, the PMF between OA and a single guest was evaluated along the central 4-fold cylindrical rotational symmetry (C_4) axis of OA (Figure 2) to form a 1:1 complex. The guests modeled were adamantane and a series of LJ solutes with diameters, σ_{ss}, varied from 3 Å to 8.5 Å in 0.5 Å increments and well depths, ε_{ss}, varied from 0.5 to 1.5 kcal/mol in 0.5 kcal/mol increments. While realistic guests may not be represented as a single LJ site, these LJ guests span sizes from slightly smaller than methane, to neopentane, adamantane, and just below the size of a buckyball. In these simulations one OA, one guest, and 1500 water molecules were explicitly considered. PMFs were evaluated over a series of overlapping windows using umbrella-sampling. The guest was restrained to the C_4 axis using a harmonic potential. In the case of adamantane, a dummy atom was created at its center to pull it along the C_4 axis. Sample windows were simulated from the center-of-mass of the aromatic rings at the bottom of OA to 21 Å (Figure 4, z = 0) into bulk solvent. Forty-three overlapping windows were considered along the C_4 axis with the harmonic umbrella potential minimum separated in 0.5 Å increments with a force constant of 5 kcal/(mol Å^2). The guests we constrained to the C_4 axis by an orthogonal harmonic force constant of 100 kcal/(mol Å^2). The C_4 axis of the cavitand similarly was aligned

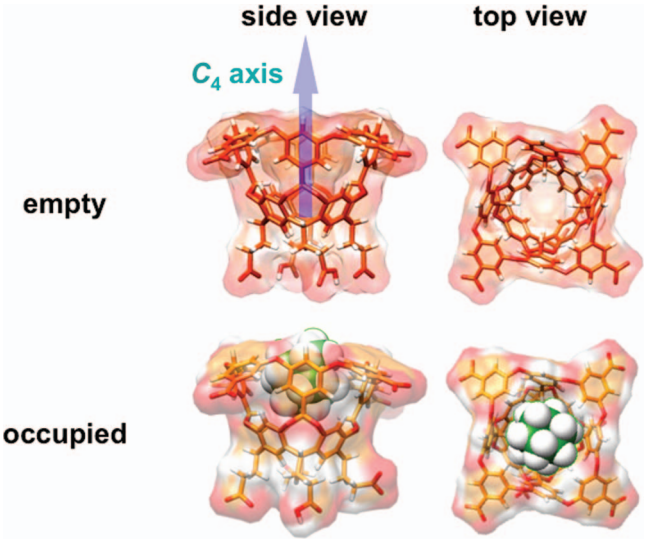

FIG. 2. Side and top views of an empty and adamantane occupied octa-acid cavitand. The cavitand is depicted as a wire frame structure encased within a transparent solvent-excluded volume, while the adamantane guest is drawn as the solid CPK structure. The C_4 axis indicated in the top left figure is the cylindrical axis that passes through OA's hydrophobic pocket that displays 4-fold rotational symmetry.

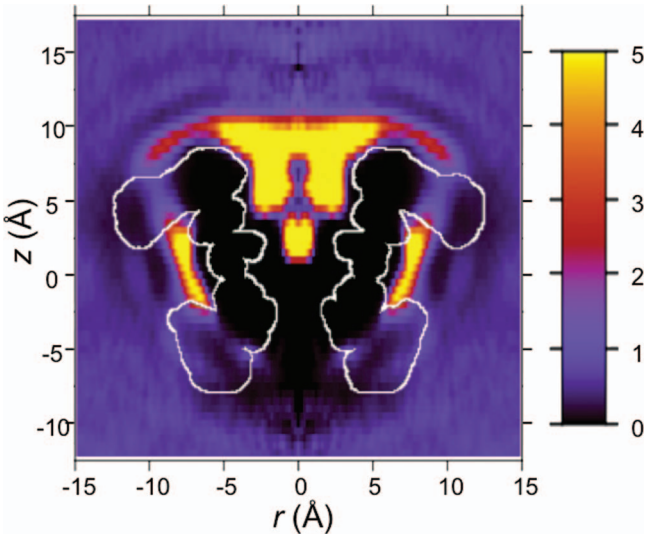

FIG. 3. Two-dimensional methane concentration distribution averaged about the C_4 axis of cavitand. The methane concentration scale shown on right-hand side of the figure has been normalized by the bulk methane concentration. Yellow indicates the positions of greatest methane adsorption, while black indicates no adsorption. An outline of the cylindrically averaged cavitand structure is overlaid in white.

along the z-axis of the simulation box using a second set of harmonic restraints that constrain the mouth of the cavitand to be fixed in space normal to the z-axis. Each simulation window was equilibrated for 2 ns and followed by a 10 ns production run. System configurations were saved every 0.2 ps. The PMF was reconstructed from the 43 windows by the weighted histogram analysis method[45] (WHAM) using the program WHAM.[46]

RESULTS AND DISCUSSION

To characterize the OA recognition pocket we initially simulated ten methanes in aqueous solution with a single host to map the binding sites of model non-polar guests. Assuming the cavitand is cylindrically symmetric about the C_4 rotational symmetry axis (Figure 2), binding to OA can be quantified by mapping the methane concentration distribution along the axial and radial directions (Figure 3). While methane weakly adheres to the cavitand exterior between the rim and foot coating groups, methane is most strongly attracted to the central hydrophobic pocket. On average 2.7 ± 0.6 methanes were found within the pocket, while the guest occupancy fluctuated between 0 and 4 methanes during the course of the simulation. The methanes predominantly sit at two positions within the pocket. One methane sits at the bottom of the cavitand pocket (indicated by the bright yellow spot centered at $z \approx 2$ Å in Figure 3) while the remaining methanes crowd around the top of the pocket and hydrophobic face of the cavitand (from $z \approx 4$ to 10 Å). While a single methane nearly continuously occupies the bottom site, the methane at the bottom frequently exchanges positions with methanes at the top of the pocket. Methanes at the top of the pocket readily escape into solution without replacement by another methane, although they may eventually be recaptured. This simulation demonstrates that unrestrained non-polar species are preferentially attracted to the cavitand pocket, and that guests with a range of sizes may be anticipated to be absorbed within the pocket given the number of methanes that can be accommodated within the pocket.

Following our assessment that the strongest non-polar guest absorption occurs within the hydrophobic pocket of OA, subsequent simulations have evaluated the PMF between OA and hydrophobic guests along the C_4 axis from the pocket interior into bulk aqueous solution. Adamantane is a nearly spherical hydrocarbon (chemical formula $C_{10}H_{16}$) with a thermal diameter of 6.1 Å that snugly fits inside the OA pocket (Figure 2). The thermal diameter is defined here as the separation at which the orientationally averaged adamantane-adamantane gas phase PMF less the value of the potential at its minimum is equal to the product of the gas constant and absolute temperature RT (i.e., $\ln\langle\exp[-\varphi(r_{\min}, \boldsymbol{\theta})/RT]\rangle_{\boldsymbol{\theta}} - \ln\langle\exp[-\varphi(r_{\text{therm}}, \boldsymbol{\theta})/RT]\rangle_{\boldsymbol{\theta}} = 1$, where θ denotes the relative adamantane-adamantane orientation, $r_{\min}$ is the position of the minimum in the gas phase PMF, and r_{therm} is the thermal diameter). The PMF between adamantane and OA exhibits a deep attractive minimum of −19.2 kcal/mol (or −32.2 RT) seated inside the hydrophobic pocket (Figure 4), effectively trapping adamantane within the cavitand after adsorption at ambient conditions. This observation stands in difference to the simulation discussed above where methanes at the top of the hydrophobic pocket were found to escape into bulk solution with relative ease. The minimum in the adamantane-cavitand PMF, corresponding to the most stable adsorption position, occurs at approximately 5.5 Å from the center-of-mass of bottom aromatic rings of the host. This minimum lies in the upper region of the pocket above the solitary methane adsorption site (Figure 3).

From an experimental perspective functionalized guests conjugated with adamantane are some of the most strongly

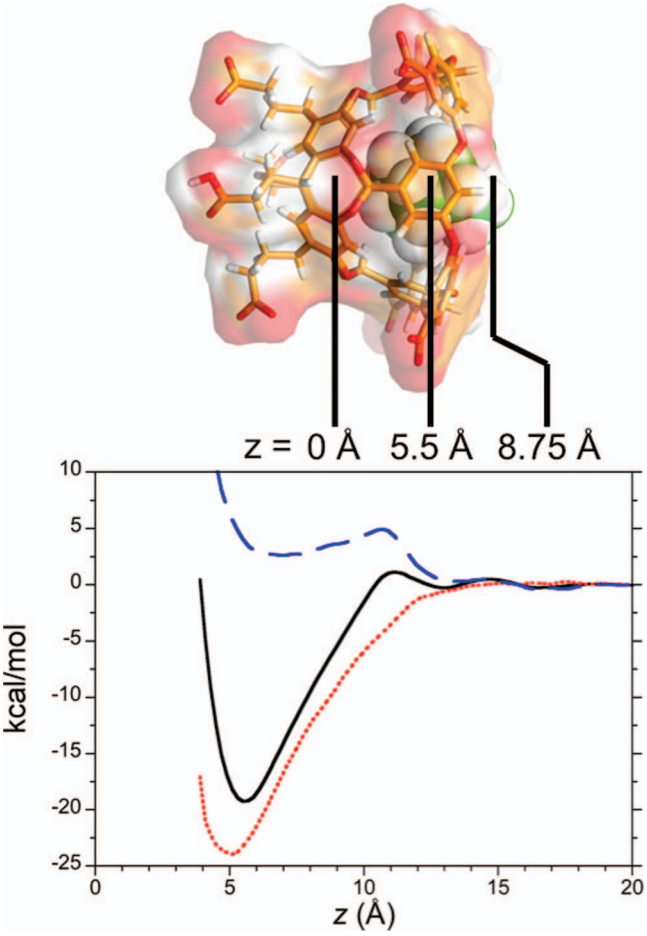

FIG. 4. Potential-of-mean force for pulling the center-of-mass of adamantane from the cavitand interior into bulk water along the C_4 axis. The total PMF is represented by a solid black line, and is decomposed into direct adamantane/cavitand interactions (dotted red line) and indirect solvent-mediated interactions (long dashed blue line). The figure above the graph illustrates the positions of the bottom of the pocket located at the center-of-mass of the lower ring of aromatic groups ($z = 0$ Å), the minimum of the potential-of-mean force between adamantane and the cavitand ($z = 5.5$ Å), and the top of the cavitand ($z = 8.75$ Å). The error bars for the potential-of-mean force computed using bootstrap analysis[46] are comparable to the plot line thickness used.

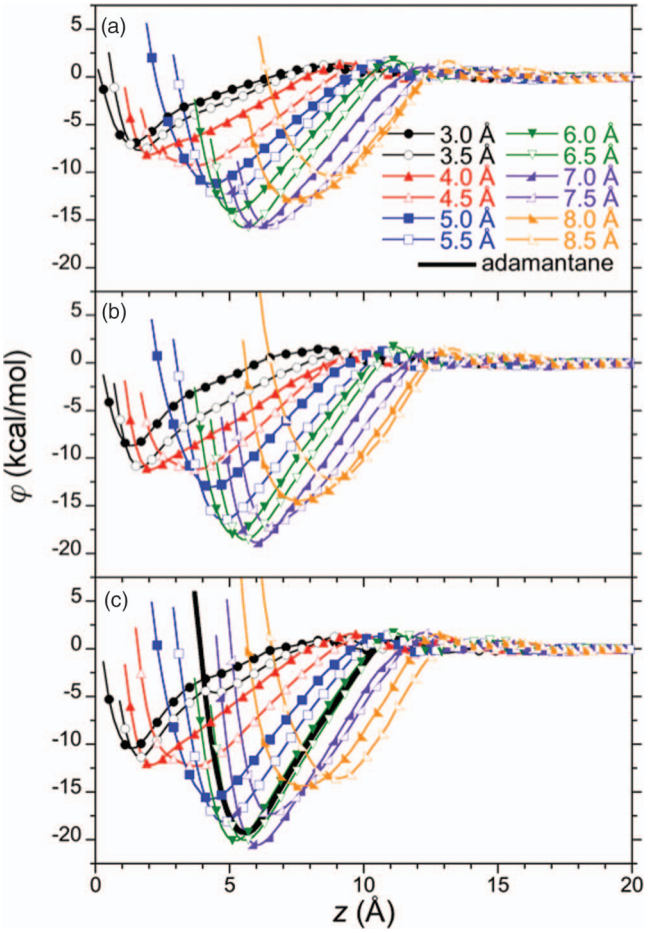

FIG. 5. Potentials-of-mean force for pulling a series of LJ guests from the cavitand interior into bulk water along the C_4 axis. The PMFs for different sized guests are identified in the figure legend. Guest diameters range from 3 Å to 8.5 Å in 0.5 Å increments, with results for guests well-depth of 0.5 kcal/mol, 1.0 kcal/mol, and 1.5 kcal/mol reported in (a), (b), and (c). The potential-of-mean force for adamantane is superimposed over the results in (c). The error bars for the potentials-of-mean force computed using bootstrap analysis[46] are comparable to the plot line thickness used.

bound species to OA.[31,32] This raises the question: What are the contributions of the guest size and attractive interactions to optimizing relative binding affinities? To this end we have evaluated PMFs along the C_4 axis for a range of LJ guests of varying diameter and well-depth (Figure 5). Not unexpectedly, the preferred guest seating depends on its size with the primary PMF minimum shifted out to increasing separation with increasing guest diameter. For a fixed guest well-depth the depth of the PMF minimum exhibits a non-monotonic dependence on the guest size. The PMF is optimally attractive for guests with diameters in the range of 6–7.5 Å, with smaller and larger guests having more shallow minima. Increasing the LJ guest well-depth largely acts to increase the magnitude of the attractive well for the PMF. We note that for the smallest guests simulated, comparable in size to methane, a 1.5 kcal/mol well-depth likely imparts significant solubility in water. Nevertheless, these smaller solutes exhibit increasing affinity for the hydrophobic binding pocket relative to water with increasing attractions. Comparing the nearly spherical adamantane with our results for LJ guests, we find the PMFs for the LJ solutes with diameters between 6 and 6.5 Å and well-depth 1.5 kcal/mol are in near quantitative agreement with the adamantane PMF (Figure 5(c)). This comparison agrees reasonably with the 6.1 Å adamantane diameter estimated from the guest thermal radius and places admantane within the range of optimally sized guests for deep-cavity recognition.

Plotting the position of the primary minimum for each PMF versus the guest diameter, we observe three distinct guest binding zones (Figure 6(a)). For the smallest diameter guests with diameters less than or equal to 4 Å, comparable in size to methane or a noble gas atom, the minimum is a linear function of the guest diameter with separations less than z_{min} = 2.5 Å (Figure 6 – zone I). This bound places these guests at the bottom of the cavitand pocket where a single methane was observed to reside in our preliminary methane simulations (Figure 3). Rather than follow the initial linear correlation, the optimal guest position jumps to greater separations between guest diameters of 4 and 4.5 Å. In this second zone

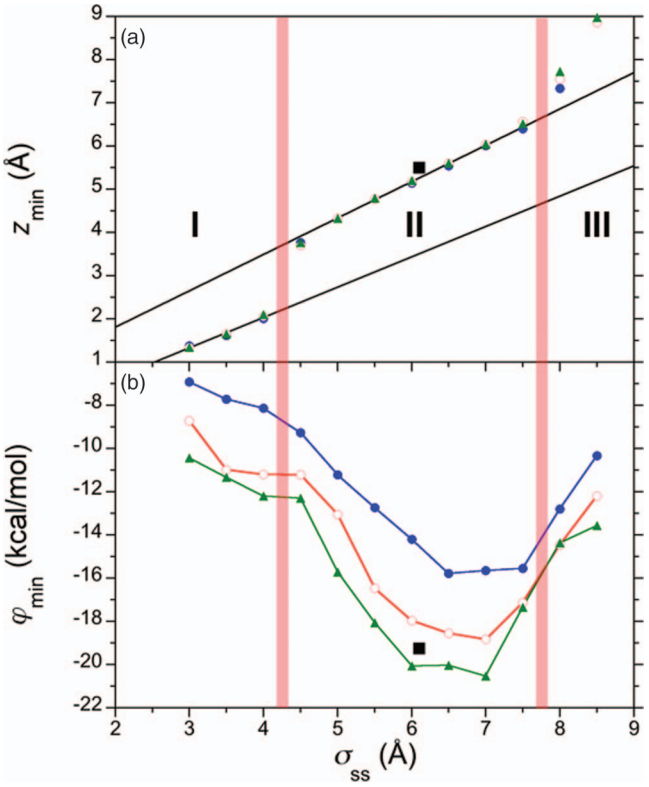

FIG. 6. Characterization of the optimal binding for the simulated guests as a function of the guest size and attractiveness. Three different binding zones (I, II, and III) were identified and demarked by the transparent red lines. (a) The position of the minimum in the simulated potentials-of-mean force along the C_4 axis as function of the LJ guest diameters. The filled blue circle, open red circles, and filled green triangles indicate results for guests with well-depths of 0.5, 1.0, and 1.5 kcal/mol, respectively, while the position of adamantane is indicated by the filled black square. The two solid straight lines indicate the linear relationships between the position of the binding minima and guest diameter in zones I and II. (b) Depth of the minimum in the potentials-of-mean force as a function of the guest diameters. The symbols follow the definitions as in (a), while the connecting lines are simply a guide to the eye.

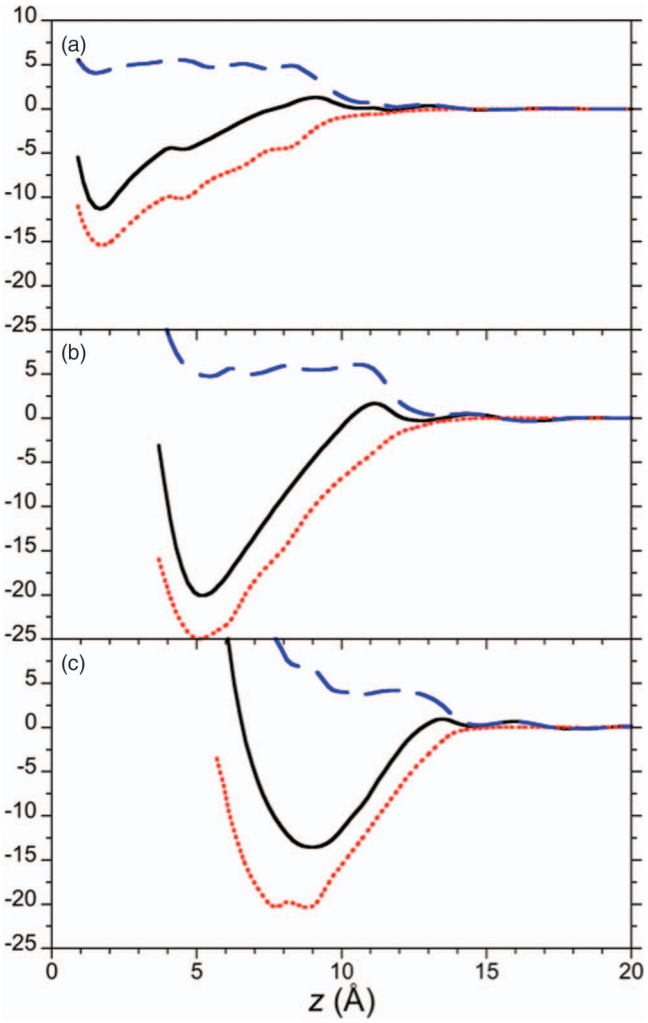

FIG. 7. Breakdown of the potentials-of-mean force into direct and indirect interactions for representative LJ guests the preferentially bind to zones I, II, and III. The solid black line, dotted red, and long dashed blue lines indicate the total potential-of-mean force, direct interaction, and indirect interaction, respectively. Figures (a), (b), and (c) report results for guests with LJ diameters of 3.5 Å (zone I), 6 Å (zone II), and 8.5 Å (zone III), respectively. The LJ well-depth of each of these guests was 1.5 kcal/mol. The error bars for the potentials-of-mean force computed using bootstrap analysis[46] are comparable to the plot line thickness used.

(zone II) for guests ranging in diameter from 4.5 to 7.5 Å, the minimum is again a linear function of guest diameter. In this regime the guests sit at optimal separations between 3 and 7 Å, placing them in the top half of the cavitand pocket where methanes were observed to freely exchange with the bulk solution (Figure 3). For guests with diameters larger than 7.5 Å, a third nonlinear binding zone (zone III) is observed at optimal guest separations even greater than those observed for the second regime. The position of the minima observed in this regime ($z_{min} > 7$ Å) places the guests outside the hydrophobic pocket and partially contacting the hydrophobic face of the cavitand.

In each binding zone we observe distinct differences in the depth of the primary PMF minimum (Figure 6(b)). In zone I for guests up to 4 Å in diameter the PMF minimum is a weakly decreasing function of guest diameter. Once the guest size crosses into zone II the decrease in the PMF well-depth becomes more significant, ultimately obtaining an optimal depth for guests ranging in diameter from ∼6 to ∼7.5 Å. The PMF well-depth increases sharply with increasing guest diameter in zone III making binding more unfavorable. As noted above, the effect of increasing the guest LJ attractions on the PMF is largely to increase the depth of the attractive well. Increasing guest attractions, on the other hand, does not significantly affect the optimal guest size. At 6.1 Å the diameter of adamantane is nearly optimal, sitting at the maximum attractiveness of zone II.

To gain insight into guest binding differences within different regions of the cavitand pocket we have broken the PMFs into direct guest-host interactions and indirect solvent-mediated contributions for adamantane and representative guests with LJ diameters of 3.5 Å, 6 Å, and 8.5 Å and well-depths of 1.5 kcal/mol that preferentially sit in zones I, II, and III, respectively (Figures 4 and 7). Here we define the direct interaction as the inter- and intramolecular potential energy of the guest and host that would be present even in vacuum. The indirect interaction is determined by the difference between the PMF and the direct contribution and captures changes in the solvent interactions with the guest, host, and other solvent

molecules. The dissection of the PMFs of adamantane (Figure 4) and the 6 Å LJ guest (Figure 7(b)) into direct and indirect interactions are in good agreement with one another, indicating the 6 Å guest is a reasonable model for rationalizing the optimal binding of adamantane. These PMFs are dominated by the direct interactions between the guests and cavitand that are even more attractive than the total free energy. The resulting indirect solvent-mediated interactions are repulsive, disfavoring adsorption. Wanjari, Sangwai, and Ashbaugh[29] observed a similarly weakly repulsive indirect interaction for alkane absorption from aqueous solution into carbon nanotube interiors. While this indirect interaction indicates water mildly opposes binding with the pocket, we found in our previous study of alkane absorption inside carbon nanotubes that the indirect solvent interaction is overwhelmingly repulsive for guest binding from organic solvents like benzene.[29] The magnitude of the indirect interaction in the present case is determined in large part by the affinity of the solvent for the negatively curved pockets and crevices of non-polar binding sites. Compared to the direct interaction, the indirect interaction is relatively featureless exhibiting an initial rise to a plateau of approximately 5 kcal/mol at the onset of interactions. This barrier to 1:1 complex formation is comparable to the free energy cost of emptying OA of water evaluated from the simulations of Ewell, Gibb, and Rick[27] (see Figure 2 of Ref. 27), suggesting cavtiand evacuation by the guest is a significant step during complex formation. In the cases of adamantane and the 6 Å and 8.5 Å diameter guests the indirect interactions appear to diverge for guest-host separations below the primary minimum. While we were unable to trace the origin of this divergence, we believe it may result from comparatively poorer sampling of interactions in the repulsive portion of the direct interaction even under the influence of the umbrella potential, or the loss of direct guest-solvent interactions as the guest is pushed into the host's excluded volume.

As noted above, the binding PMFs are dominated by the direct guest-host interaction. In the case of the 3.5 Å, 6 Å, and 8.5 Å guests the minimum values of the direct interactions are −15 kcal/mol, −25 kcal/mol, and −20 kcal/mol, respectively (Figure 7). These minima mirror the variation in the depth of the PMFs with increasing guest size (Figure 6(b)). The deeper direct interaction of the 6 Å guest compared to the 3.5 Å guest results from the larger number of neighboring host atoms available for the medium-sized guest to interact with in the upper binding region of the pocket (zone II) compared to that of the small-sized guest at the bottom of the pocket (zone I). Similarly the deeper direct interaction of the 6 Å guest compared to the 8.5 Å guest results from the comparatively greater number of neighboring atoms available to the medium-sized guest in the upper binding region compared to that of the large-sized guest which does not fit through the portal of the cavitand and sits on the OA face (zone III).

Approximately four water molecules sit within the OA pocket in the absence of a bound guest (Figure 8), consistent with the results of Ewell, Gibb, and Rick.[27] When a guest approaches the cavitand portal the number of waters in the pocket drop precipitously. In the case of the 6 Å and 8.5 Å LJ guests all the waters spontaneously evacuate the cavitand and

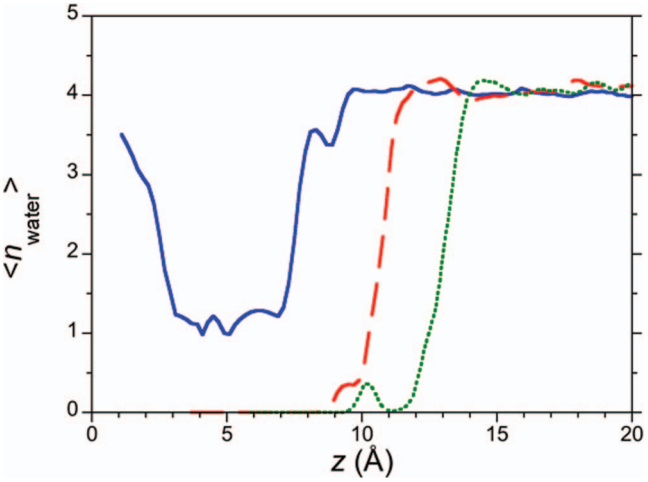

FIG. 8. Average number of water molecules present inside the cavitand pocket as a function of guest separation. The solid blue, long-dashed red, and dotted green lines indicate results for LJ guest diameters of 3.5 Å, 6 Å, and 8.5 Å, respectively. The LJ well-depth of each of these guests was 1.5 kcal/mol.

the occupancy falls to zero when these solutes arrive at the pocket entrance, consistent with the solvent-mediated barrier to complex formation discussed above. The drop in water occupancy of the pocket coincides with the onset of the guest-host interactions in the PMF (Figure 7) suggesting the repulsive nature of the indirect interactions results in part from lost favorable interactions between the solvent and cavitand interior. In the case of the 3.5 Å guest, the pocket occupation is reduced from four to one water molecules left inside when the guest arrives at the cavitand mouth. As the small guest comes to rest at the primary minimum of the PMF at a separation of ∼1.5 Å water refills the pocket resulting in a final average water occupancy between 3 and 4 waters. Experimentally only *n*-alkanes longer than methane form stable complexes with OA. Moreover, Ewell, Gibb, and Rick[27] observed from simulations that ethane induces complete OA evacuation. Since the small guest examined here is comparable in size to the OPLS united-atom description of methane, it may be inferred that complete desolvation of the cavitand pocket plays a significant role in the formation of stable guest-host complexes.

CONCLUSIONS

In summary, molecular simulations of simple non-polar solutes and OA deep cavity cavitands in water were performed to evaluate the relative contributions of molecular size and attractiveness to optimizing hydrophobic guest binding within the binding pocket of the cavitand. While methane weakly binds to sites on the cavitand exterior, the strongest binding was observed within the cavitand pocket. Despite being strongly attracted to the pocket, the total methane population within the cavitand fluctuated over the course of our 50 ns simulation with methanes escaping and exchanging with solutes in the bulk solution. This simulation highlighted two binding regions within the cavitand: one at the bottom of the hydrophobic pocket big enough for a single methane, and

a second at the top in the mouth of the cavitand where multiple methanes can sit and exchange with the bulk solution.

Subsequent simulations to evaluate the PMFs between LJ guests and the hydrophobic cavitand pocket along the central axis demonstrated that the site at which a single guest preferentially sits is determined by the guest size. Guests comparable in size to methane preferentially sit in the bottom region, while guests successively migrate to the cavitand portal and ultimately the cavitand face with increasing diameter. The strongest interactions were observed for guests ranging in diameter from 6 to 7.5 Å that bind in the main binding chamber of the binding site (zone II), while smaller and larger guests exhibited weaker binding. Over the range of LJ guest well-depths simulated attractive guest interactions predominantly affected the binding strength, but not the preferential binding region or size selectivity. These observations are consistent with the experimental observation that adamantane and its derivatives are some of the strongest cavitand binding guests. In the case of adamantane derivatives with side chain groups, entropic penalties resulting from the loss of tumbling degrees-of-freedom inside the pocket will accompany guest-host complexation. Nevertheless, adamantane pendant groups can potentially gain additional interactions that further stabilize complex formation either by pointing the derivative unit toward the cavitand bottom or out towards the bulk solution to interact with the host face.

While water readily wets the cavitand pocket, which accommodates four waters molecules on average, the water occupation state within the pocket rapidly fluctuates on the simulation time scale. The waters within readily evacuate the pocket when a hydrophobic guest is brought to the cavitand face, leaving zero to one waters left inside depending on the guest size. As a result water makes a repulsive contribution to the non-polar guest-host PMF. The net attractive guest/host interaction free energy is thereby dominated by the direct attractive van der Waals interaction. The 6–7.5 Å diameter guests enjoy the strongest binding as a result of the greater number of neighboring cavitand atoms the medium-sized guests can interact within the cavitand throat, compared to the smaller number of neighbors small guests have in the bottom of the cavitand or the reduced set of neighbors large guests have on the cavitand face. From this perspective, optimization of non-polar guest binding relies on maximizing guest-host contact area to gain van der Waals attractions.

ACKNOWLEDGMENTS

H.S.A. and P.P.W. acknowledge support from the Louisiana Board of Regents PKSFI program who provided financial support for this project and from the Louisiana Optical Network Initiative who provided computational support. B.C.G. acknowledges support from the National Institutes of Health (No. GM074031).

[1]C. L. D. Gibb and B. C. Gibb, J. Am. Chem. Soc. **126**, 11408–11409 (2004).
[2]S. Liu, S. E. Whisenhunt-loup, C. L. D. Gibb, and B. C. Gibb, Supramol. Chem. **23**, 480–485 (2011).
[3]C. L. D. Gibb, E. D. Stevens, and B. C. Gibb, J. Am. Chem. Soc. **123**, 5849–5850 (2001).
[4]S. Liu and B. C. Gibb, Chem. Commun. (Cambridge) **2008**, 3709–3716.
[5]L. S. Kaanumalle, C. L. D. Gibb, B. C. Gibb, and V. Ramamurthy, J. Am. Chem. Soc. **126**, 14366–14367 (2004).
[6]A. Natarajan, L. S. Kaanumalle, S. Jockusch, C. L. D. Gibb, B. C. Gibb, N. J. Turro, and V. Ramamurthy, J. Am. Chem. Soc. **129**, 4132–4133 (2007).
[7]C. L. D. Gibb, A. K. Sundaresan, V. Ramamurthy, and B. C. Gibb, J. Am. Chem. Soc. **130**, 4069–4080 (2008).
[8]C. L. D. Gibb and B. C. Gibb, J. Am. Chem. Soc. **128**, 16498–16499 (2006).
[9]S. Liu, H. Gan, A. T. Hermann, S. W. Rick, and B. C. Gibb, Nat. Chem. **2**, 847–852 (2010).
[10]D. Podkoscielny, C. L. D. Gibb, B. C. Gibb, and A. E. Kaifer, Chem.-Eur. J. **14**, 4704–4710 (2008).
[11]A. Baldridge, S. R. Samanta, N. Jayaraj, V. Ramamurthy, and L. M. Tolbert, J. Am. Chem. Soc. **132**, 1498–1499 (2010).
[12]A. Baldridge, S. R. Samanta, N. Jayaraj, V. Ramamurthy, and L. M. Tolbert, J. Am. Chem. Soc. **133**, 712–715 (2011).
[13]M. Porel, S. Jockusch, A. Parthasarathy, V. J. Rao, N. J. Turro, and V. Ramamurthy, Chem. Commun. (Cambridge) **48**, 2710–2712 (2012).
[14]J. Y.-C. Chen, N. Jayaraj, S. Jockusch, M. F. Ottaviani, V. Ramamurthy, and N. J. Turro, J. Am. Chem. Soc. **130**, 7206–7207 (2008).
[15]H. Sun, C. L. D. Gibb, and B. C. Gibb, Supramol. Chem. **20**, 141–147 (2008).
[16]C. L. D. Gibb and B. C. Gibb, J. Am. Chem. Soc. **133**, 7344–7347 (2011).
[17]G. Hummer, Nat. Chem. **2**, 906–907 (2010).
[18]P. W. Snyder, J. Mecinovic, D. T. Moustakas, S. W. Thomas, M. Harder, E. T. Mack, M. R. Lockett, A. Heroux, W. Sherman, and G. M. Whitesides, Proc. Natl. Acad. Sci. U.S.A. **108**, 17889–17894 (2011).
[19]J. Qvist, M. Davidovic, D. Hamelberg, and B. Halle, Proc. Natl. Acad. Sci. U.S.A. **105**, 6296–6301 (2008).
[20]D. E. Smith and A. D. J. Haymet, J. Chem. Phys. **98**, 6445–6454 (1993).
[21]T. Ghosh, A. E. Garcia, and S. Garde, J. Chem. Phys. **116**, 2480–2486 (2002).
[22]S. W. Rick, J. Phys. Chem. B **104**, 6884–6888 (2000).
[23]E. Sobolewski, M. Makowski, C. Czaplewski, A. Liwo, S. Oldziej, and H. A. Scheraga, J. Phys. Chem. B **111**, 10765–10774 (2007).
[24]R. Baron, P. Setny, and J. A. McCammon, J. Am. Chem. Soc. **132**, 12091–12097 (2010).
[25]P. Setny, R. Baron, and J. A. McCammon, J. Chem. Theory Comput. **6**, 2866–2871 (2010).
[26]P. Setny, Z. Wang, L. T. Cheng, B. Li, J. A. McCammon, and J. Dzubiella, Phys. Rev. Lett. **103**, 187801 (2009).
[27]J. Ewell, B. C. Gibb, and S. W. Rick, J. Phys. Chem. B **112**, 10272–10279 (2008).
[28]G. Hummer, J. C. Rasaiah, and J. P. Noworyta, Nature (London) **414**, 188–190 (2001).
[29]P. P. Wanjari, A. V. Sangwai, and H. S. Ashbaugh, Phys. Chem. Chem. Phys. **14**, 2702–2709 (2012).
[30]A. Kalra, G. Hummer, and S. Garde, J. Phys. Chem. B **108**, 544–549 (2004).
[31]Z. R. Laughrey, C. L. D. Gibb, and B. C. Gibb, Chem.-Eur. J. **9**, 130–139 (2003).
[32]C. L. D. Gibb, H. Xi, P. A. Politer, M. Concha, and B. C. Gibb, Tetrahedron **58**, 673–681 (2002).
[33]D. Frenkel and B. Smit, *Understanding Molecular Simulation: From Algorithms to Applications*, 2nd ed., (Academic Press, San Diego, 2001).
[34]B. Hess, C. Kutzner, D. van der Spoel, and E. Lindahl, J. Chem. Theory Comput. **4**, 435–447 (2008).
[35]H. W. Horn, W. C. Swope, J. W. Pitera, J. D. Madura, T. J. Dick, G. L. Hura, and R. Head-Gordon, J. Chem. Phys. **120**, 9665–9678 (2004).
[36]J. Wang, R. M. Wolf, J. W. Caldwell, P. A. Kollman, and D. A. Case, J. Comput. Chem. **25**, 1157–1174 (2004).
[37]M. J. Frisch, G. W. Trucks, H. B. Schlegel *et al.*, Gaussian 03, Revision C.01, Gaussian, Inc., Wallingford, CT, 2004.
[38]D. A. Case, T. A. Darden, T. E. Cheatham III, C. L. Simmerling, J. Wang, R. E. Duke, R. Luo, K. M. Merz, D. A. Pearlman, M. Crowley, R. C. Walker, W. Zhang, B. Wang, S. Hayik, A. Roitberg, G. Seabra, K. F. Wong, F. Paesani, X. Wu, S. Brozell, V. Tsui, H. Gohlke, L. Yang, C. Tan, J. Mongan, V. Hornak, G. Cui, P. Beroza, D. H. Mathews, C. Schafmeister, W. S. Ross, and P. A. Kollman, AMBER 9 (University of California, San Francisco, 2006).
[39]T. Darden, D. York, and L. Pedersen, J. Chem. Phys. **98**, 10089–10092 (1993).

[40]S. Nose, J. Chem. Phys. **81**, 511–519 (1984).
[41]W. G. Hoover, Phys. Rev. A **31**, 1695–1697 (1985).
[42]M. Parrinello and A. Rahman, J. Appl. Phys. **52**, 7182–7190 (1981).
[43]B. Hess, H. Bekker, H. J. C. Berendsen, and J. E. G. M. Fraaije, J. Comput. Chem. **18**, 1463–1472 (1997).
[44]W. L. Jorgensen, J. D. Madura, and C. J. Swenson, J. Am. Chem. Soc. **106**, 6638–6646 (1984).
[45]S. Kumar, D. Bouzida, R. H. Swendsen, P. A. Kollman, and J. M. Rosenberg, J. Comput. Chem. **13**, 1011–1021 (1992).
[46]A. Grossfield, WHAM: the weighted histogram analysis method, version 2.0.7, University of Rochester, 2013.